J Solid State Electrochem (2005) 9: 371–379
DOI 10.1007/s10008-004-0642-6

ORIGINAL PAPER

L. M. Plyasova · I. Yu. Molina · G. N. Kustova
N. A. Rudina · M. I. Borzenko
G. A. Tsirlina · O. A. Petrii

Solid state features of electrocrystallized tungstate films

Received: 28 September 2004 / Revised: 1 December 2004 / Accepted: 3 December 2004 / Published online: 15 February 2005

Abstract X-ray diffraction, scanning electron microscopy, and infra-red spectroscopy are applied to study the evolution of films electrodeposited from acidic tungstate solutions. Structural inhomogeneity is found to be responsible for the difference in rechargeability of films of different thickness. Voltammetric responses demonstrate pronounced sensitivity to the nature of crystalline phases, thus throwing light on the defects of the lattice features of nonstoichiometric W(V)–W(VI) oxides. One crystalline phase observed in the films under study and attributed to the layered nonstoichiometric oxohydroxide was never reported for oxotungstate films fabricated by other techniques. This phase is believed to be special to electrocrystallized films and to keep some structural features of dissolved isopolytungstate molecular precursors.

Keywords Tungsten oxide · Nonstoichiometric · Electrocrystallization · Crystal structure

Introduction

Formation of solid products in the process of anions' electroreduction is a phenomenon typical of various oxygen-containing compounds of transition metals. One of the most intriguing examples, which attracted attention to this problem, was observed by Horanyi's school for chromate species in acidic medium [1]. We report below, a study of the nature of similar tungstate films whose precursors are isopolytungstate anions existing in long-lived metastable acidic solutions [2, 3].

Excellent electrochromic properties of various hydrated tungsten oxides are widely discussed in the literature in relation to their structure, and key points in these discussions are usually to do with the nature of precursors and fabrication techniques [4–16]. Earlier, we mentioned some nucleation manifestations [2, 3, 17] which gave a basis to consider the deposition process as a type of cathodic electrocrystallization. This paper is devoted to more direct study of films' crystallinity and its evolution. Despite the rechargeable films under study having specific properties, which are of interest for various applications, the presented system can be considered as a model system for understanding the structural interplay of dissolved species and solid products of their electroreduction in the context of recharging ability.

Materials and methods

The reagents $Na_2WO_4{\cdot}2H_2O$ and 18 M H_2SO_4 were of analysis grade quality (Merck). Twice-distilled water was additionally purified on a Milli-Q setup. Preparation of the long-lived sulfuric acid-supported solutions of isopolytungstates (containing mainly isopolyanions $[W_7O_{24}]^{6-}$ and $[W_{10}O_{32}]^{4-}$) is described in detail in [2, 3, 17]. A possibility to stabilize W(VI) in acid by using similar procedure was reported earlier, but any solutions used by other authors to deposit solid WO_x were always prepared by a different technique, namely metallic W dissolution in H_2O_2-containing acid [4].

The films were deposited on etched (aqua regia) Pt foil, under potential cycling within the interval 0.05–1.1 V (here and below, the potential E_r is reported in the scale of reversible hydrogen electrode (RHE) in the 0.5 M H_2SO_4 supporting solution.). A three-electrode

Dedicated to Prof. G.Horanyi with the highest respect to his experimental talents, remarkable papers and important contributions in various fields of modern electrochemistry.

L. M. Plyasova · I. Yu. Molina · G. N. Kustova
N. A. Rudina
Boreskov Institute of Catalysis,
Siberian Branch of the Russian Academy of Sciences,
Novosibirsk, Russia

M. I. Borzenko · G. A. Tsirlina (✉) · O. A. Petrii
Department of Electrochemistry, Moscow State University,
Moscow, Russia
E-mail: tsir@elch.chem.msu.su

cell with separated compartments and Autolab PGSTAT30 (Eco Chemie) were always used for potential cycling in the course of deposition and subsequent electrochemical characterization in the supporting solution. In the latter case, stabilized voltammetric responses were already observed within the second–fourth cycle.

To avoid the formation of insoluble tungstic acid in the course of deposition, with its subsequent electrophoretic codeposition, the polarization was interrupted any time between 1.5 h and 2 h, and solution was replaced by a fresh portion. After deposition from the last portion the films were thoroughly washed by Milli-Q water. Prior to X-ray diffraction (XRD), scanning electron microscopy (SEM), and infra-red spectroscopy (IR) experiments, the films were dried in air. Aging also took place in air.

The estimated thicknesses of the films were 1, 2, and 3 μm. The thicknesses were estimated from the values of charge taking into account our previous data on the reduction degree and total charge, which agreed with the preceding scanning tunnelling microscopy (STM) thickness estimates (possible for thin films only) [2, 3]. It was found to be proportional to the cycle number, which is rather natural because the lack of reagent during the rather short deposition period between the change for new portion never exceeded several percent. For comparative experiments, electrophoretic deposition of colloidal tungstic acid was done under the same mode. Colloidal deposition solution was obtained by room temperature aging of the usual metastable deposition solution. It was started at the free support surface after colloid formation, when the residual concentration of isopolyanions in the solution became negligible. In contrast to electrocrystallization, for which the thickness always increased with the cycle number, the thickness of electrophoretic film reached a limit and could not be additionally increased by changing the colloidal solution. Determining the reason for this self-inhibition and the exact values of electrophoretic film thickness are beyond the scope of this study because these samples are used only for qualitative comparison.

The XRD patterns were recorded using diffractometers URD-63 (Freiberger—Mechanik), D-500 (Siemens), and D-8 (Bruker) with the Cu K_α radiation. To cut off the K_α component, a graphite monochromator was used in the reflected beam. The recording was done in the angle interval 2θ varying over the interval 5–40° with a step of 0.02–0.05° and accumulation time of 5–10 s. The $K_{\alpha 1}$ constituent was isolated. The JCPDS database [18] was used for references. PCW software [19] was applied for modeling the theoretical XRD patterns. SEM images were obtained with a LEO1430 device standardized by using 50 A test sample.

Diffuse reflectance IR spectra in the region 500–4,000 cm^{-1} were collected using Shimadzu FTIR-8300 spectrometer with diffuse reflectance supplement DRS-8000. Electrochemical tests before and after any characterization series were arranged in the usual manner [2, 3] in supporting 0.5 M H_2SO_4 solution.

A sample of yellow tungstic acid used for comparison was prepared by slowly adding a solution of sodium tungstate (3 g $Na_2WO_4 \cdot 2H_2O$ in 30 ml of water) to 12 M HCl (6 ml) while stirring. Thus obtained gel was thoroughly washed with water and dried in air at room temperature.

XRD examination of the phase composition: evidence of layered phase formation

The most detailed XRD study was accomplished using 3-μm film whose XRD response demonstrated crystallinity features immediately after deposition. For thinner films, as-deposited samples appeared X-ray amorphous. We attribute these manifestations to a high initial content of nanocrystalline or amorphous phases whose content can depend on the film thickness. Nanostructured fragments (5–7 nm) in the films under discussion were found earlier by STM in the sample of submicron thickness.

X-ray diffraction manifestations of aging at room temperature (additional reflections) appeared after 1.5 months (compare curves 1 and 2 in Fig. 1). No qualitative changes of phase composition were observed in the course of further aging for another 2.5 months (curve 3 in Fig. 1).

For as-deposited samples, all reflections can be attributed to several phases [18] (Table 1), but identification remains slightly uncertain because of a limited number of reflections. Assignment based on the assumption of tungsten–bronze formation cannot be excluded. However, these phases are evidently minor. Assignment of a number of reflections to Na_2WO_4 should be considered as conditional because Na_2WO_4 is initially introduced as the reagent but can be hardly

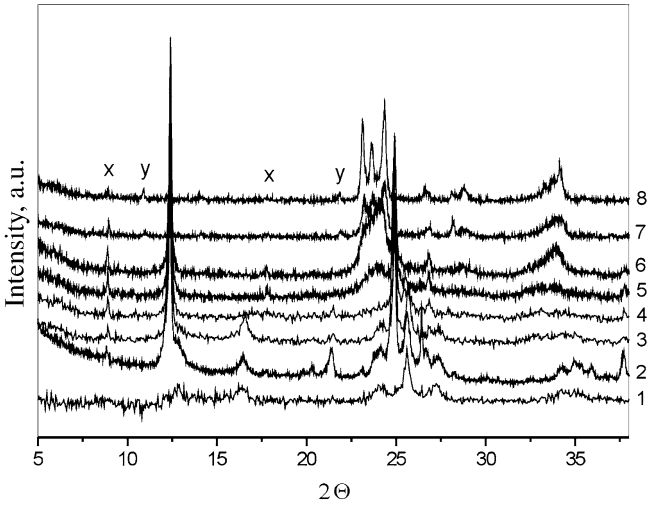

Fig. 1 X-ray diffraction patterns of the electrocrystallized film: *1* as-deposited, *2, 3* aged in air at room temperature (1.5 and 4 months respectively), *4–8* annealed at 150 (4), 300 (5), 400 (6), 500 (7), 600 °C (8). *X* and *Y* correspond to assignment discussed in the text as related to Fig. 4

Table 1 Assignment of experimentally observed interatomic distances (d, Å) for as-deposited (pattern 1, Fig. 1) and room-temperature aged (patterns 2, 3, Fig. 1) samples

As-deposited	Aged	$WO_3 \cdot H_2O$ (H_2WO_4)(43–0679)	$H_2WO_4 \cdot H_2O$ (18–1420)	$MeO_{3-x}OH_x$ (Me = W)[a]	Na_2WO_4 (20–1163)
	10.03				
–	7.15			7.15	
6.93	6.97		6.96		
5.40	5.39	5.36			
	5.01				5.02
	4.37				
–	4.15				4.12
–	3.84				
–	3.73	3.73	3.77		
3.70					
3.69	3.70			3.70	
–	3.58			3.58	
3.48	3.46	3.46	3.47		
–	3.37			3.37	3.37
–	3.33		3.31		
3.27	3.25		3.26		
	3.16				3.18
					3.08, 3.07
					2.874
2.788					
				2.966	
2.62	2.61	2.616	2.648	2.656	2.688
			2.627	2.610	
2.56	2.56	2.555	2.545		2.535
	2.5				
	2.38			2.363	
	2.34				
–	2.30				

A number of less intensive reflections can be also refereed [18] to various tungsten bronzes, for example $H_{0.1}WO_3 \cdot 1.06H_2O$ (40–0694, 23–1448), $H_{0.12}WO_3 \cdot 2H_2O$ (40–0693), $H_{0.23}WO_3$ (42–1261)

[a]Structure refinement on the basis of [22]

crystallized from diluted solutions. The absence or presence of this phase is not crucial for the complete assignment of observed XRD patterns.

Figure 2 demonstrates that the experimental pattern for the as-deposited sample can be presented by combination of patterns for H_2WO_4 (theoretical) and $H_2WO_4 \cdot H_2O$ (measured for bulk sample; large cell volume of hydrated tungstic acid and very high number of atoms in the cell complicate the calculation of theoretical pattern.) The latter is a single phase solid with XRD parameters identical to JCPSD [18, No. 18–1420]. This comparison gives direct evidence of the coexistence of two tungstic acid phases of different hydration degrees, but also does not exclude the presence of partly reduced protonated phases.

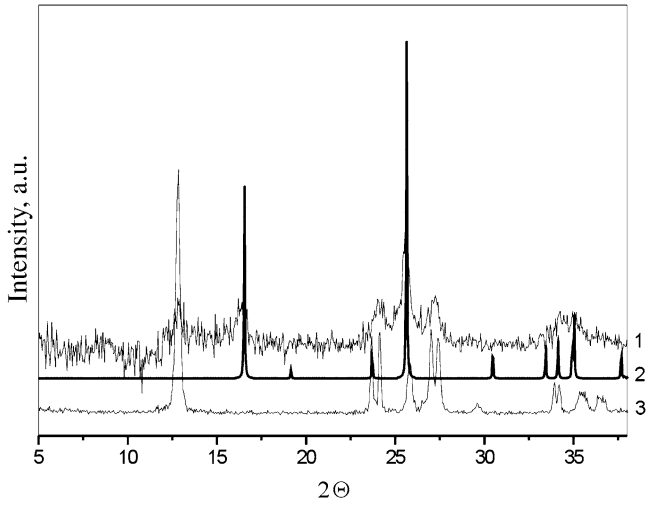

Fig. 2 XRD patterns of as deposited electrocrystallized film (1) as compared to the calculated spectra for H_2WO_4 (2) and (3) experimental pattern of yellow tungstic acid $H_2WO_4 \cdot H_2O$

New reflections resulting from aging (Fig. 1, curve 2) cannot be related to any of the phases found in as-deposited sample. The most intensive of them are multiple, and correspond to interplanar distances $d = 7.15$ and 3.58 Å, which fact favors an assumption of preferential orientation of the newly formed phase (typical for layered oxocompounds [20]).

No oxotungstates or hydroxotungstates demonstrating the above-mentioned d values were found in the databases. Taking into account the well-known structural similarity of W and Mo oxocompounds [21] we made a search of analogs and concluded that the observed reflections can be assigned to a tungsten-based relative of the layered $MoO_{3-x}(OH)_x$ [18, JCPDS, No. 34–1230, 70–0615]. According to [22], the latter structure can be considered as the derivative of ReO_3 (the same structural type is known for WO_3). Each layer consists of top-connected MoO_6 octahedrons that are linked into double layer packages via edges. Typical features of these layered hydroxides are as follows: partial protonation of oxygen atoms, existence of appropriate (5+) metal atoms, and location of water molecules in the interlaminar areas. Idealized structure of the type described in [22] is portrayed in Fig. 3.

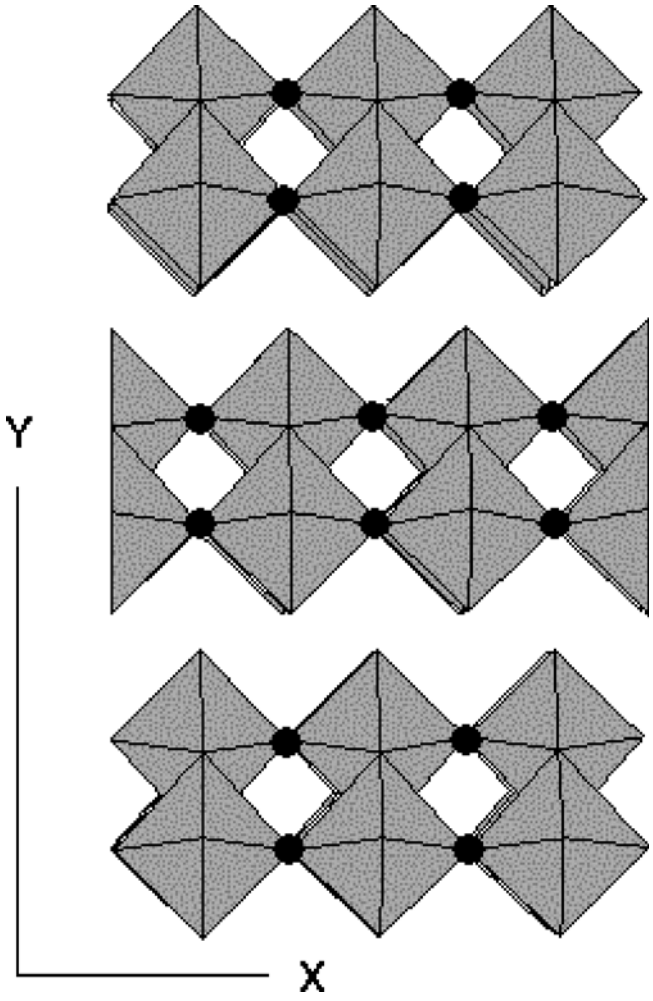

Fig. 3 Idealized structure of $WO_{3-x}(OH)_x$

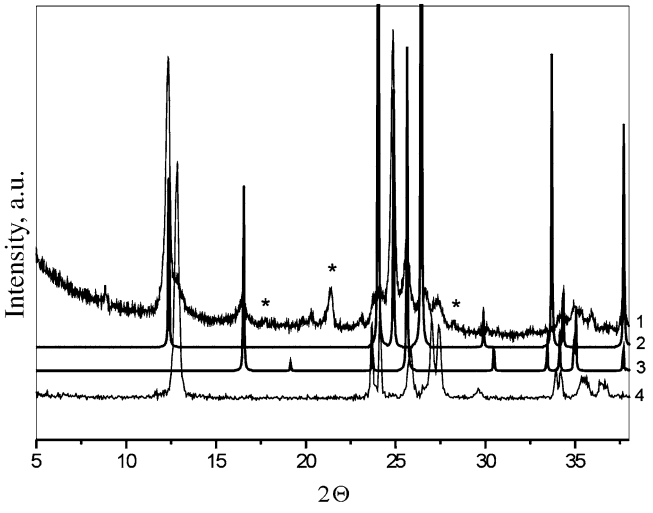

Fig. 4 XRD pattern of the electrocrystallized film aged in air at room temperature (1) as compared to calculated spectra for $WO_{3-x}(OH)_x$ (2), H_2WO_4 (3) and $H_2WO_4{\cdot}H_2O$ (4). Spectrum (2) corresponds to *Pbnm* space group (**a** = 3.80 Å, **b** = 14.25 Å, **c** = 3.79 Å)

Figure 4 presents the comparison of the experimental pattern for room-temperature aged sample (curve 1) with the calculated pattern (2) for hypothetical $WO_{3-x}(OH)_x$ phase. The latter results from structure refinement on the basis of [22], and corresponds to *Pbnm* space group with parameters $a = 3.80$ Å, $b = 14.25$ Å, $c = 3.79$ Å. Curves 3 and 4 in Fig. 4 correspond to H_2WO_4 and $H_2WO_4{\cdot}H_2O$, respectively. It is evident from this figure that the predominating components of aged film are three phases, namely, two types of tungstic acid, which were already found in the as-deposited film, and an additional layered protonated compound, which either formed in the course of aging or attained better crystallinity in the course of aging. The latter hypothesis seems to be more realistic because the appearance of layered phase is not accompanied by disappearance of the initially existing tungstic acid(s).

To observe further phase evolution, a set of XRD patterns was obtained after subsequent annealing at various temperatures increasing in series from 150 °C to 600 °C (patterns 4–8, Fig. 1). Both tungstic acid phases disappeared after the first annealing at 150 °C, when the reflections corresponding to $d = 7.15$ and 3.58 Å remained unchanged up to 400 °C (patterns 4–6 in Fig. 1). These reflections disappear at higher temperatures. Simultaneously, new oxide phas(es), WO_3 and/or H_xWO_3, start to form at 300 °C: two broad reflections (pattern 5 in Fig. 1) are attributed to the most intensive reflections of cubic tungsten oxide (or cubic tungsten bronze). Dehydrated tungsten oxide of high crystallinity is observed after annealing at 500–600 °C (patterns 7, 8 in Fig. 1). Comparison of these data with the pattern for triclinic WO_3 (Fig. 5) demonstrates good agreement.

Some reflections of low intensity (see asterisks in Fig. 4) can result from decreased symmetry of the $WO_{3-x}(OH)_x$ phase, the more detailed structural description of which requires special future examination. A limited number of experimental reflections in combination with texture and reflections overlap in the multiphase sample, complicate this study. The data obtained for annealed samples, however, indicate that the weak reflections ($d = 5.02$, 4.15, 3.37 Å) cannot be assigned either to Na_2WO_4 or to layered $WO_{3-x}(OH)_x$ (because of their disappearance in the course of annealing at already 150 °C). There are also weak multiple reflections which can be attributed to disordered layered structures with interlaminar distances of $d = 10.03$ and 8.12 Å (and corresponding $d = 5.00$ and 4.07 Å). The reflections under discussion are conditionally attributed, in Fig. 1, to phases *X* and *Y*. Phase *X* manifests itself in all observed patterns excluding the as-deposited sample, whereas phase *Y* appears only after high-temperature treatment (patterns 7 and 8 in Fig. 1).

A comparative study of annealed thinner sample (Fig. 6), which initially demonstrated no crystallinity, confirms that the appearance of layered phase with relatively high thermal stability is typical of the electrodeposited films under study and does not depend crucially on the film thickness. An interesting feature found in this

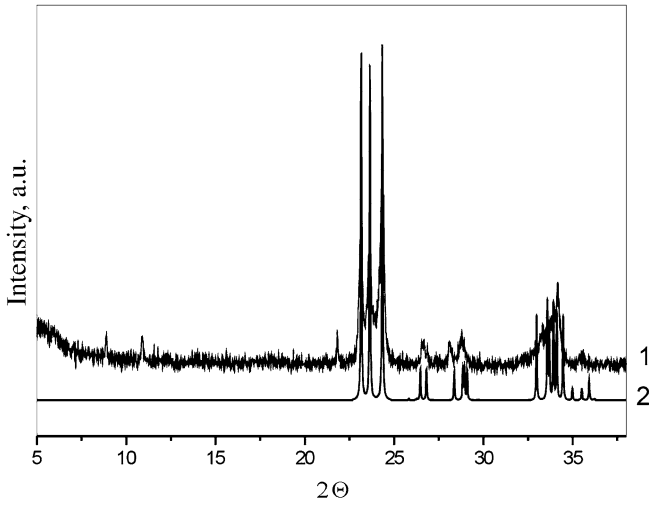

Fig. 5 XRD pattern of the electrocrystallized film annealed at 600 °C (1) as compared to calculated spectra (2) of triclinic WO_3

series of experiments was the slow appearance of $WO_{3-x}(OH)_x$ in the sample (see asterisks), which was completely transformed to triclinic WO_3 at 600 °C. This result demonstrates that, in contrast to unusual layered phase, triclinic WO_3 is metastable in moist air at room temperature.

A film formed from electrophoretically deposited colloid demonstrated no crystallinity features. This film was rather thin (certainly < 1 μm), and its XRD patterns after both aging and annealing gave no chance for unambiguous interpretation. We should stress that the increase of deposition time does not result in higher thickness of colloid-based film.

Morphological versus structural evolution

Figure 7 presents a set of representative SEM images of the sample, whose structural evolution is described in the previous section. Figure 7a (as-deposited sample) demonstrated a complex morphology whose main features are columnar tumors covered by coalesced crystals of 0.1–1 μm size. Much smaller fragments are visible along the flat regions of the surface. Taking into account the XRD data reported above, it appears reasonable to connect these crystals to two phases of tungstic acids and to assume that amorphous or nanocrystalline XRD-

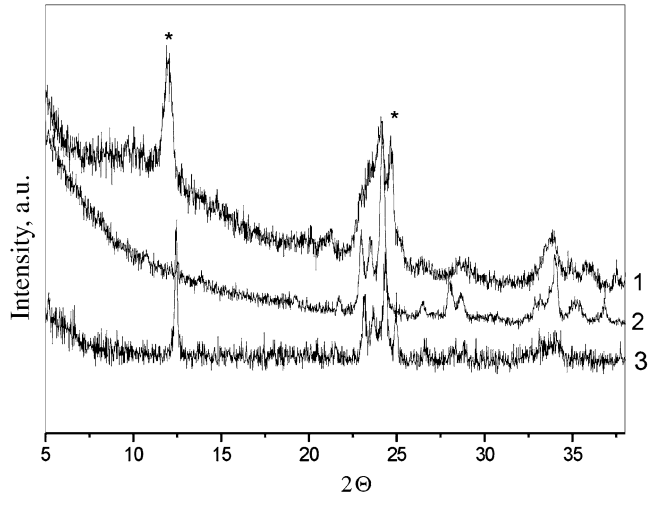

Fig. 6 XRD patterns of thinner film annealed at 400 °C (1), 600 °C (2), and (3) kept in air for 15 days

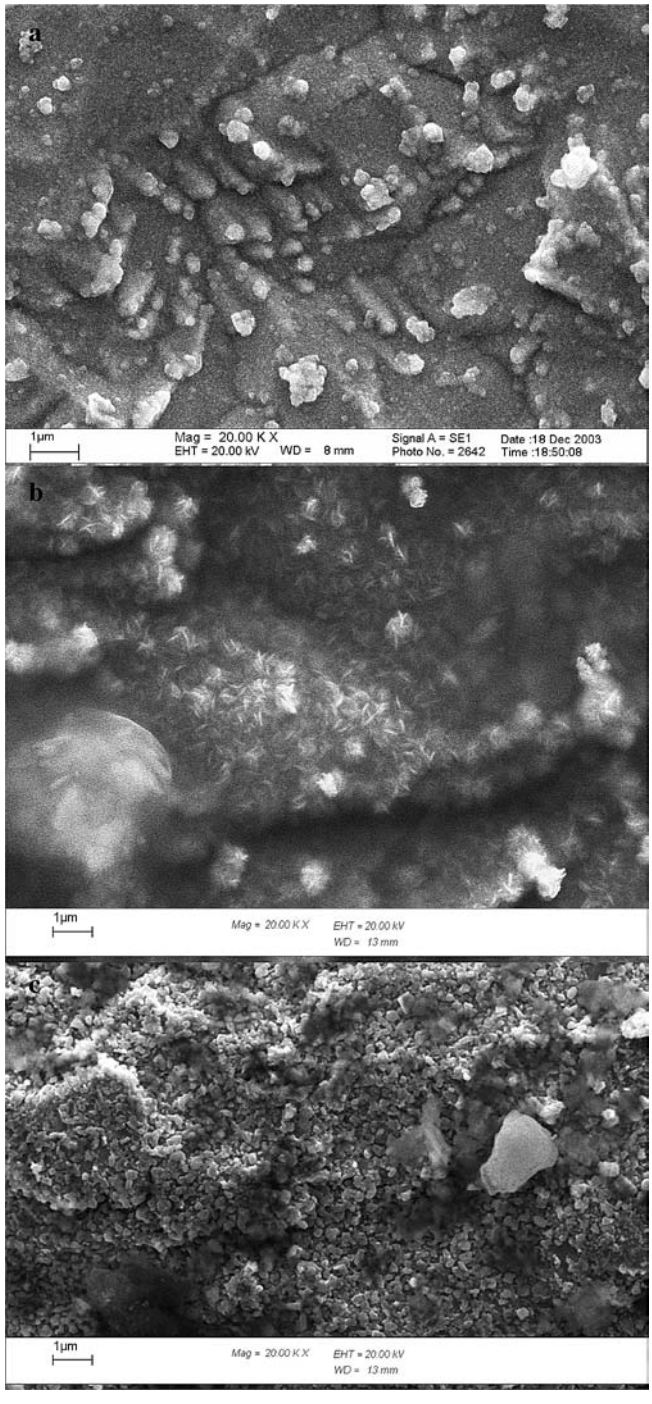

Fig. 7 SEM images of the tungstate films: *1* as deposited, *2* aged in air at room temperature, *3* annealed at 600 °C

invisible components of the solid form the less-structured sublayer.

The pronounced difference between as-deposited and aged samples consists in the appearance of needle-like crystals in the course of aging (Fig. 7b). These needles are ca. 0.5 μm in length and <0.1 μm in diameter. Such morphology is rather probable for oriented growth of the layered phase assumed above (needle-shaped habitus and tendency to texture formation are typical of layered structures of MoO_3 type). For the needle-like structure, the [0*k*0] type reflections become most evident in diffraction patterns. So the XRD pattern evolution with aging time (Fig. 1) can be associated with an increase in ordering of layers in the [0*k*0] direction. As a result of increase in texturing in [0*k*0] direction, the intensities of reflections in other directions decrease.

The morphology of the annealed sample (Fig. 7c for heat treatment at 600 °C) agrees with high crystallinity. Submicron-size crystals (0.1–0.2 μm) are distributed all over the surface, and no fragments of another shape are visible. Basically, the SEM data are in good agreement with XRD-based scheme of films evolution under aging and annealing.

IR manifestation of dehydration processes

The spectral features of the films under study are rather complex, and at this stage we avoid complete assignment of the observed bands. The main goal of IR spectroscopy is to correlate the observed structural and morphological differences with some molecular features of tungstates, tungsten oxides, and their hydrates. For all as-deposited films under study, three characteristic regions can be noted (Fig. 8).

Less-resolved bands in the 600–1,100 cm^{-1} spectral region are assigned to tungsten–oxygen vibrations. A number of observed bands were previously described for hydrated tungstic acid [23] (bands in the vicinity of 700 cm^{-1}, and also at 930, 1,004, 3,195, 3,384, 3,528 cm^{-1}). According to [24], bands at 635 and 950 cm^{-1} are typical of H_2WO_4. There are also some bands in this region that are similar to specific vibrations in various isopolytungstates [25, 26] (770–870 cm^{-1} region).

The bands at 1,420–1,440 cm^{-1} should be assigned to carbonate ions resulting from the contact with air. Other bands in this intermediate spectral region are related to water deformation vibrations (1,620–1,640 cm^{-1}) and hydronium ion (1,700–1,765 cm^{-1}) [27, 28]. The pronounced hydration is confirmed by the well-resolved bands above 3,200 cm^{-1}, which correspond to stretching vibrations.

Figure 8 demonstrates that the exact spectral features depend on the film thickness. There are also some similarities between electrophoretically deposited colloid (spectrum 4) and thin electrodeposited films (spectra 1 and 2 in Fig. 8), but these films are far from being identical. The absence of a band at 3,750 cm^{-1} for the thicker film reveals its partial dehydration even before prolonged aging, i.e. dehydration can take place in the course of more prolonged growth. Difference in spectral features related to various isopolytungstates manifests in the fact that some solution equilibria with participation of these precursors continue to shift in the course of deposition, which is rather natural for metastable systems.

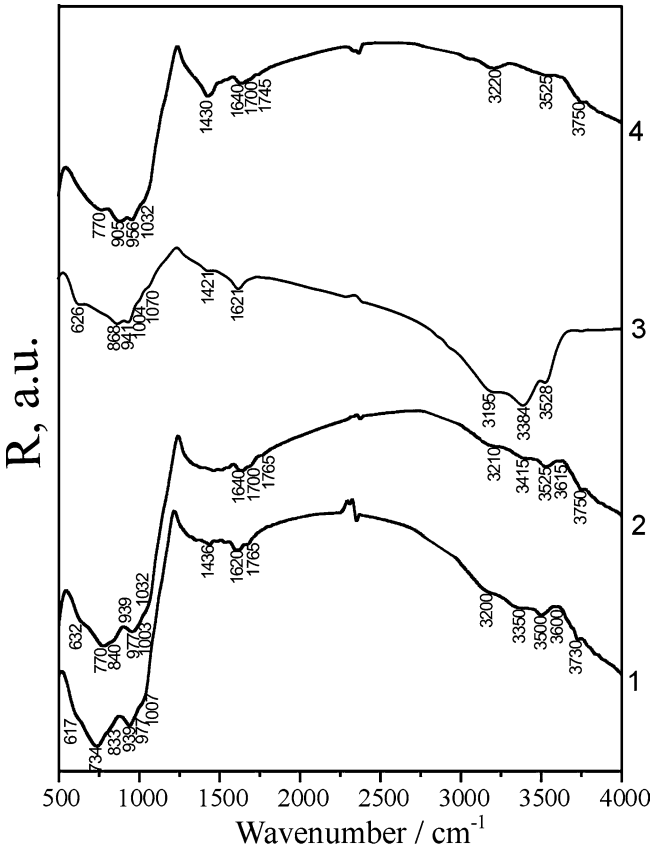

Fig. 8 IR reflection spectra of freshly deposited films of various thicknesses (numbers of curves correspond to thickness, μm). Spectrum for electrophoretically deposited colloid of tungstic acid (4) is given for comparison

The most illustrative IR observations are obtained for the films' evolution in the course of thermal treatment (Fig. 9a). The spectrum of the film heated at 150 °C (curve 2) demonstrates pronounced, but still incomplete, dehydration (the vicinity of 1,700 cm^{-1} and the region above 3,200 cm^{-1}). In parallel, the evolution of spectra in the region below 1,100 cm^{-1} takes place. Bands at 693 and 1,100 cm^{-1} appear, which can be assigned to $WO_{3-x}(OH)_x$ because of the similarity with the spectra for layered molybdenium analog [22].

Annealing at higher temperatures (300 and 400 °C, curves 3 and 4 in Fig. 9a) demonstrates less-pronounced spectral changes. Stability of spectra in the temperature region for which the existence of layered phase was assumed from XRD data favors an assignment of a large set of bands in curves 2–4 (Fig. 9a) to crystalline WO_3.

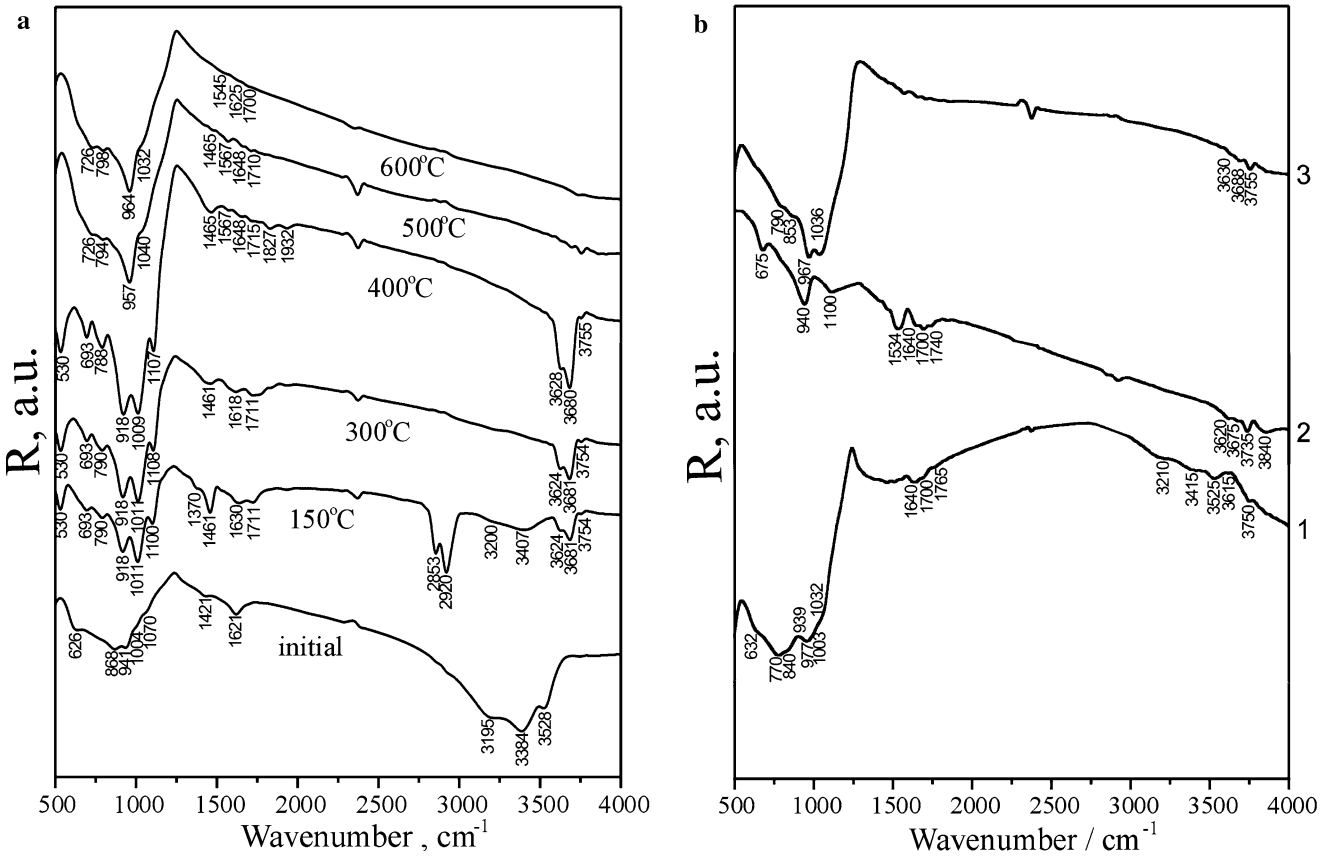

Fig. 9 IR reflection spectra of the thick tungstate film **a** *1* as-deposited; *2–6* annealed at 150 (*2*), 300 (*3*), 400 (*4*), 500 (*5*) and 600 °C (*6*). **b** Comparative data for as-deposited (*1*), annealed (*2*, at 600 °C) and room temperature aged (*3*) thinner films

$_x(OH)_x$. In contrast, spectra 5 and 6 in Fig. 9a (registered after annealing at 500 and 600 °C, respectively) confirm complete dehydration (disappearance of bands at ca. 1,700 cm^{-1} and in the region above 3,200 cm^{-1}), with simultaneous formation of less simple patterns at lower frequencies. This spectrum is very close, but not identical, to the spectrum of tungsten oxide reported in [28], and demonstrates similarity with a spectrum of molybdenium bronze [29].

Figure 9b demonstrates the changes in IR spectra that correspond to structural transformations of thin film illustrated by XRD patterns in Fig. 6 (2, 3). Again, we observe a correlation between both techniques, which favors the attributing of bands and reflections to one and the same phase, assumed to be $WO_{3-x}(OH)_x$.

A number of bands described below were observed in our previous in situ Raman study of thin films [17]. In particular, a band at 977 cm^{-1} can be related to W(5+)–O vibration (981 cm^{-1} in [17]), which demonstrated potential dependence. The existence of the residual W(5+) in the films kept in air for a long time presents the most surprising fact and confirms that the structural features of nonstoichiometric hydrated oxides can strongly affect the regions of stability of the lower oxidation states.

Electrochemical manifestations of films' solid state composition

Typical cyclic voltammograms (CV) of the films under study are collected in Fig. 10. Current values are normalized per film thickness and geometric surface area. For freshly deposited films and films aged at room temperature, no serious dependence of CV features on the thickness was found for scan rates 5–20 mV s^{-1}. At higher scan rates, aged films demonstrate the decrease of total capacity induced by charge transport limitations inside the film [3]. For fresh films, these limitations appeared at scan rates >50–100 mV s^{-1}. Typical CV behavior observed before annealing is illustrated in Fig. 10a. There are at least three coalesced peaks, which most probably correspond to the film fragments of different crystal structure. It is difficult to compare the responses in Fig. 10 with any voltammograms presented in the literature because, usually, more deep reduction (more negative potential limit) is applied for the films on non-platinum supports.

Changes in electrochemical behavior induced by annealing are rather strong and depend on the film thickness. Total charge decreases, and the rechargeability potential region becomes more narrow. Decrease of charge with the scan rate increase manifests slower charge transport in the films.

For thinner film (Fig. 10b) these changes are less dramatic, and several recharging processes can be still

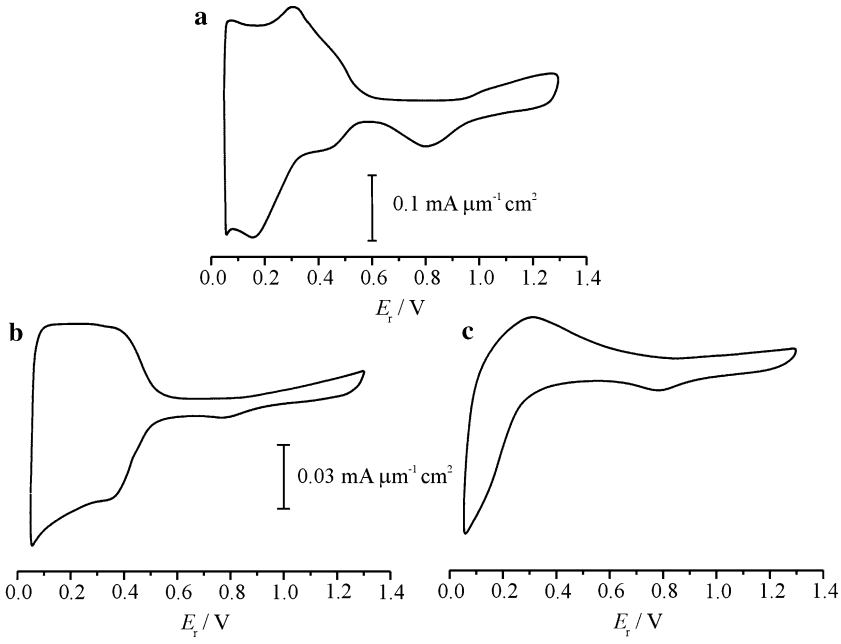

Fig. 10 Typical stabilized cyclic voltammograms of as-deposited **a** and annealed (**b, c**, at 600 °C) films. The currents are normalized per film thickness and geometric surface area. Curve **a** is typical for all films before annealing, both fresh and aged. Curves **b** and **c** correspond to 1 and 3 μm film thickness, respectively. All data are presented for scan rate 20 mV s^{-1}

noticed, which form a wide, square anodic maximum. The charge spent for the cathodic scan remains higher than the charge spent for the subsequent anodic scan. This means that the equilibrium state of the solid under study requires the reduction, which is slow under cycling conditions. One can assume that the upper layers of the film undergo fast hydration and reduction in the course of several initial scans and later demonstrate quasi-reversible charge–discharge, whereas a portion of deeper located substance still requires hydration/reduction. This assumption agrees with capacity decrease as compared to initial value. It also explains why (Fig. 10c) such decrease is more pronounced for the thicker film, and reversibility is very poor.

Voltammetric feature at 0.45–0.55 V, always observed for freshly deposited and room temperature aged films (Fig. 10a, [2, 3]), is absent in the curves of annealed films. Taking into account XRD data discussed above, we can attribute this feature to a newly found layered phase.

Conclusions

The results of this study confirm the important role of interlayer water in the transport of protons which accompanies the electrochemical recharging processes. As for the former one, we can suggest that at various potential regions the specific recharging processes of different solid phases occur. Actually, the widest recharging region is observed for freshly deposited films of the most complex phase composition, whereas the narrowest and simplest response is found for the less complex annealed film. A special study of the effects of temperature on electrochemical responses and evaluation of the electrochemistry of layered $WO_{3-x}(OH)_x$ are in progress.

Observations of solid state evolution presented in this paper on the basis of XRD, SEM, and IR spectroscopy data are reviewed in Fig. 11. It demonstrates the subsequent transformations of isopolyanions existing in

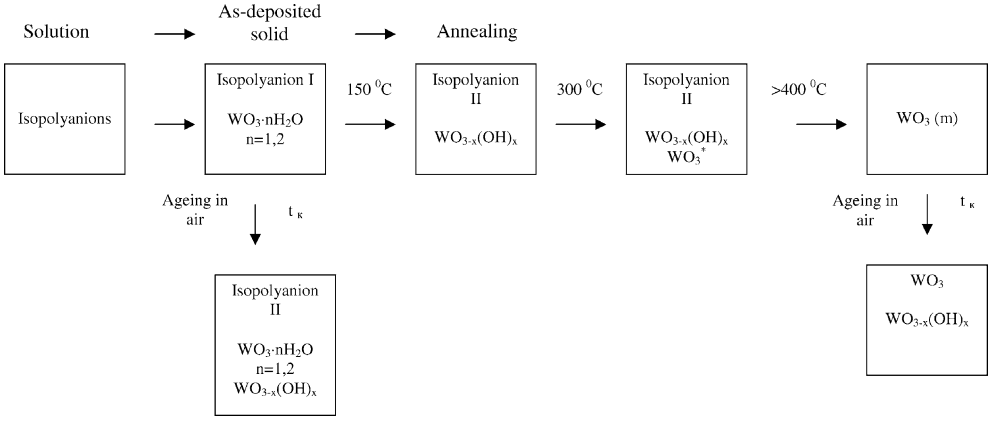

Fig. 11 Schematically represented structural evolution of the electrodeposited solid

deposition solution, which accompanies the structural evolution of the film in the course of room temperature aging and heat treatment. We should stress that the presence of the layered $WO_{3-x}(OH)_x$ phase grounded above is unique to earlier studies of electrochromic tungsten oxide films (see, for example [4, 23, 28]). Our qualitative explanation of its appearance is the possibility to form specific structures in the course of the electrocrystallization process, with the participation of dissolved isopolyanions.

We would like to mention also the analogy with formation of nonstoichiometric molybdenium oxides [30–32] whose structural and stoichiometric features (including mixed oxidation state) attainable at various temperatures in the region 200–500 °C are strongly dependent on the synthesis technique and precursor nature. It seems like the phenomena described in this paper are typical of oxygen compounds of transition metals.

Acknowledgements The authors are grateful to P.V. Berdnikova for providing a sample of yellow tungstic acid. We also acknowledge the financial support of RFBR (project 04-03-33055a) and the Council for Grants of President of Russian Federation for leading scientific schools (NSh-2089.2003.3). G.A.T is grateful to RSSF.

References

1. Inzelt G, Horanyi G (1999) J Electroanal Chem 471:73
2. Timofeeva EV, Tsirlina GA, Petrii OA (2003) Russ J Electrochem 39:716
3. Timofeeva EV, Borzenko MI, Tsirlina GA, Astaf'ev EA, Petrii OA (2004) J Solid State Electrochem 8:778
4. Granqvist CG (2000) Solar Energy Mater Solar Cells 60:201
5. Guery C, Choquet C, Dujeancourt F, Tarascon JM, Lassegues JC (1997) J Solid State Electrochem 1(3):199
6. Bohnke O, Vuellemin B, Gabrielli C, Keddam M, Perrot H, Takenouti H, Torresi R (1995) Electrochim Acta 40:2755
7. Denesuk M, Uhlmann DR (2000) Solar Energy Mater Solar Cells 62:335
8. Nishide T (1995) Thin Solid Films 259:212
9. Barreca D, Bozza S, Carta G, Rossetto G, Tondello E, Zanella P (2003) Surf Sci 532–535:439
10. Antonik M, Schneider JE (1995) Thin Solid Films 256:247
11. Ozer N (1997) Thin Solid Films 304:310
12. Wang H, Zhang M, Yang S, Zhao L, Ding L (1996) Solar Energy Mater Solar Cells 43:345
13. Daniel MF, Desbat B, Lassegues JC, Garie R (1988) J Solid State Chem 73:127
14. Paul J-L, Lassegues JC (1993) J Solid State Chem 106:357
15. Opara-Krasovec U, Jese R, Orel B, Gradolnik J, Drazic G (2002) Monatsh Chem 133:1115
16. Opara-Krasovec U, Surca Vuk A, Orel B (2001) Electrochim Acta 46:1921
17. Palys B, Borzenko MI, Tsirlina GA, Jackowska K, Timofeeva EV, Petrii OA (2005) Electrochim Acta 50:7–8
18. JCPDS (2000) PC-Powder diffraction file. Swarthmore
19. Kraus W, Nolze G (1998) CPD Newslett 20:27
20. Taylor HFW (1973) Mineralog Mag 39:377
21. Poraj-Koshits MA, Atovmyan LO (1974) Crystallochemistry and stereochemistry of coordination molybdenium compounds. Nauka, Moscow (in Russian)
22. Schroeder FA, Weitzel H (1977) Z Anorg Allg Chem 435:247
23. Li YM, Hibino M, Miyayania M, Kudo T (2000) Solid State Ionics 134:271
24. Sadtler Research Laboratories (1965) High resolution spectra of inorganics related compounds, Philadelphia, Penna, Y250
25. Rocchiccioli-Deltcheff C, Thouvenot R, Franck R (1976) Spectrochim Acta 32A:587
26. Himeno S, Yoshihara M, Maekawa M (2000) Inorg Chim Acta 298:165
27. Gillard RD, Wilkinson G (1964) J Chem Soc 5:1641
28. Balazsi CS, Farkas-Jahnke M, Kotsis I, Petras L, Pfeifer J (2001) Solid State Ionics 141–142: 411
29. Wang L, Schindler J, Kannewurf CR, Kanatzidis MG (1997) J Mater Chem 7:1277
30. Mikhailenko EA, Aleshina GI, Tarasova DV, Perkovskii Ya, Kustova GN, Ravilov RG, Olenkova IP (1982) Izvestiya SO An USSR, Seriya Chim Nauk 2:86 (in Russian)
31. Olenkova IP, Chumachenko NN, Plyasova LM, Yurchenko EN (1983) React Kinet Catal Lett 22:339
32. Olenkova IP, Chumachenko NN, Plyasova LM, Tarasova DV (1988) Z Neorg Khimii 33:1169 (in Russian)